Relative Position and Attitude Control for Drag-Free Satellite with Prescribed Performance and Actuator Saturation

TAO Jiawei, *ZHANG Tao**

Department of Automation, Tsinghua University, Beijing 100084, P. R. China

(Received 1 April 2018; revised 9 May 2018; accepted 30 May 2018)

Abstract: An adaptive prescribed performance control scheme is proposed for the drag free satellite in the presence of actuator saturation and external disturbances. The relative translation and rotation dynamics between the test mass and outer satellite are firstly derived. To guarantee prescribed performance bounds on the transient and steady control errors of relative states, a performance constrained control law is formulated with an error transformed function. In addition, the requirements to know the system parameters and the upper bound of the external disturbance in advance have been eliminated by adaptive updating technique. A command filter is concurrently used to overcome the problem of explosion of complexity inherent in the backstepping control design. Subsequently, a novel auxiliary system is constructed to compensate the adverse effects of the actuator saturation constrains. It is proved that all signals in the closed-loop system are ultimately bounded and prescribed performance of relative position and attitude control errors are guaranteed. Finally, numerical simulation results are given to demonstrate the effectiveness of the proposed approach.

Key words: relative position and attitude control; drag-free satellite; command filter; prescribed performance; actuator saturation

CLC number: V448.22 **Document code:** A **Article ID:** 1005-1120(2019)04-0617-11

0 Introduction

The drag-free satellite acts a pivotal part in many science missions including the test of equivalence principle, the detection of gravitational waves and the measurement of the earth gravity field. Pugh[1] firstly proposed drag-free concept, then it was studied systematically by Lange[2]. Specifically, the great application prospects and importance of drag-free flight have been gradually shown in many missions such as the MICROSCOPE satellite[3], the satellite test of the equivalence principle (STEP)[4-5], the gravity probe B (GP-B) satellite[6-7], the laser interferometer space antenna (LISA) satellite[8], the LISA Pathfinder satellite[9], the gravity field and ocean circulation explorer (GOCE) satellite[10-11] and so on.

The drag-free satellite contains a cavity in which a test mass is shielded by the surrounding spacecraft against the external environment disturbances. This structure provides a free-falling environment for the inside floating test mass, and the key technology is to control the outer spacecraft to chase the test mass in its purely gravitational motion. With the development of drag-free missions, a wide variety of studies about the drag-free control have been carried out.

Some control techniques including PID which lacks explicit disturbance rejection and H_∞/H_2[12-13] have been treated to design drag-free control scheme.

The model predictive control method was adopted to tackle the drag free control problem of GOCE satellite[14], where the plant's six degrees of freedom had to be decoupled into four linearized sys-

*Corresponding author, E-mail address: taozhang@tsinghua.edu.cn.

How to cite this article: TAO Jiawei, ZHANG Tao. Relative Position and Attitude Control for Drag-Free Satellite with Prescribed Performance and Actuator Saturation[J]. Transactions of Nanjing University of Aeronautics and Astronautics, 2019, 36(4):617-627.

http://dx.doi.org/10.16356/j.1005-1120.2019.04.008

tems.

A robust controller based on a simplified uncertain design plant with given structure for a plant describing a drag-free satellite was developed[15]. The designed optimal single-input-single-output controllers can robustly achieve the desired level of performance.

The Embedded Model Control (EMC) technique[16] was proposed by Canuto and then investigated to resolve the drag-free and attitude control problem of GOCE satellite[17]. The core of this control design and algorithm was the embedded model which defines three interconnected parts including the controllable dynamics, the disturbance class to be rejected and the neglected dynamics.

A control strategy that used the on-orbit time-dependent change in angle of attack for a new type of super-low-altitude flight was developed[18]. This partial drag-free flight had potential applications in some stealth military missions.

Although many schemes as mentioned above have been presented for the drag-free control design, it is always assumed that the couplings among the different degrees of freedom are highly reduced or treating them as unknown disturbance. Nevertheless, it is important to note that the behavior between the test mass and outer satellite can be regarded as a formation. The relative position and attitude are mutually coupled, especially for drag-free satellite with cubic test mass, because the relative attitude motion between the test mass and the outer satellite can be neglected for drag-free satellite with spherical test mass; besides, the thrust control system is the key unit to achieve drag-free flight by providing a precise compensation for the disturbing force except gravity. The performance of a new cusped field thruster was tested and analyzed[19], then a drag-free control scheme based on the cusped field thruster was designed to evaluate the performance of this thruster. The thruster limitation effect is a potential problem for control system design. It often severely deteriorates system performance, even leads to undesirable inaccuracy or instability.

In this paper, the integrated relative position and attitude motion between the cubic test mass and outer satellite is firstly derived. Taking model parameters uncertainty, external environment disturbance and actuator saturation into consideration, an integrated position and attitude control strategy with prescribed performance is designed by integrating adaptive technique, command filter, anti-wind technique and prescribed performance control theory. During the control design, the requirements to know the accurate system parameters and upper bound of the external disturbance are eliminated, and the tedious analytic computations of time derivatives of virtual control laws are canceled. It is proved that the proposed control can guarantee the prescribed performance of the relative position and attitude irrespective the presence of actuator saturation.

1 Mathematical Model and Problem Formulation

In this section, in order to realize precise tracking of test mass in a drag-free satellite, the dynamics of the relative motion between the test mass and the outer satellite is derived.

Considering the displacement mode of drag-free satellite with single cubic test mass, the relative attitude kinematics can be expressed as[20]

$$\dot{\boldsymbol{\sigma}}_{\mathrm{e}}=\boldsymbol{G}(\boldsymbol{\sigma}_{\mathrm{e}})\boldsymbol{\omega}_{\mathrm{e}} \tag{1}$$

$$\boldsymbol{G}(\boldsymbol{\sigma}_{\mathrm{e}})=\frac{1}{4}\left[(1-\boldsymbol{\sigma}_{\mathrm{e}}^{\mathrm{T}}\boldsymbol{\sigma}_{\mathrm{e}})\boldsymbol{I}_3+2\boldsymbol{S}(\boldsymbol{\sigma}_{\mathrm{e}})+2\boldsymbol{\sigma}_{\mathrm{e}}\boldsymbol{\sigma}_{\mathrm{e}}^{\mathrm{T}}\right] \tag{2}$$

where $\boldsymbol{\sigma}_{\mathrm{e}}$ is the modified rodrigues parameters (MRP) vector representing the relative attitude between the test mass and the outer satellite, and $\boldsymbol{\omega}_{\mathrm{e}}=\boldsymbol{\omega}_{\mathrm{s}}-\boldsymbol{R}(\boldsymbol{\sigma}_{\mathrm{e}})\boldsymbol{\omega}_{\mathrm{t}}$ is the relative angular velocity between outer satellite body frame F_{s} and the test mass body frame F_{t} expressed in frame F_{t}. The rotation matrix from F_{s} to $\mathscr{F}_{\mathrm{t}}$ is

$$\boldsymbol{R}(\boldsymbol{\sigma}_{\mathrm{e}})=\boldsymbol{I}_3-\frac{4(1-\boldsymbol{\sigma}_{\mathrm{e}}^{\mathrm{T}}\boldsymbol{\sigma}_{\mathrm{e}})}{(1+\boldsymbol{\sigma}_{\mathrm{e}}^{\mathrm{T}}\boldsymbol{\sigma}_{\mathrm{e}})^2}\boldsymbol{S}(\boldsymbol{\sigma}_{\mathrm{e}})+\frac{8\boldsymbol{S}^2(\boldsymbol{\sigma}_{\mathrm{e}})}{(1+\boldsymbol{\sigma}_{\mathrm{e}}^{\mathrm{T}}\boldsymbol{\sigma}_{\mathrm{e}})^2} \tag{3}$$

Further, the relative attitude dynamic can be governed by[21]

$$\boldsymbol{J}\dot{\boldsymbol{\omega}}_{\mathrm{e}}=\boldsymbol{C}_{\mathrm{a}}\boldsymbol{\omega}_{\mathrm{e}}+\boldsymbol{h}_{\mathrm{a}}+\boldsymbol{\tau}+\boldsymbol{\tau}_{\mathrm{d}} \tag{4}$$

where skew symmetric matrix $\boldsymbol{C}_{\mathrm{a}}$ and nonlinear term $\boldsymbol{h}_{\mathrm{a}}$ are expanded as

$$\begin{aligned}\boldsymbol{C}_{\mathrm{a}}=\boldsymbol{S}(\boldsymbol{J}(\boldsymbol{\omega}_{\mathrm{e}}+\boldsymbol{R}(\boldsymbol{\sigma}_{\mathrm{e}})\boldsymbol{\omega}_{\mathrm{t}}))-\boldsymbol{S}(\boldsymbol{R}(\boldsymbol{\sigma}_{\mathrm{e}})\boldsymbol{\omega}_{\mathrm{t}})\boldsymbol{J}-\\ \boldsymbol{J}\boldsymbol{S}(\boldsymbol{R}(\boldsymbol{\sigma}_{\mathrm{e}})\boldsymbol{\omega}_{\mathrm{t}})\end{aligned} \tag{5}$$

and

$$\boldsymbol{h}_{\mathrm{a}}=-\boldsymbol{S}(\boldsymbol{R}(\boldsymbol{\sigma}_{\mathrm{e}})\boldsymbol{\omega}_{\mathrm{t}})\boldsymbol{J}\boldsymbol{R}(\boldsymbol{\sigma}_{\mathrm{e}})\boldsymbol{\omega}_{\mathrm{t}}-\boldsymbol{J}\boldsymbol{R}(\boldsymbol{\sigma}_{\mathrm{e}})\dot{\boldsymbol{\omega}}_{\mathrm{t}} \tag{6}$$

The relative position vector between frame F_{s} and frame F_{t} is denoted as

$$\boldsymbol{r}_{\mathrm{e}}=\boldsymbol{r}_{\mathrm{s}}-\boldsymbol{R}(\boldsymbol{\sigma}_{\mathrm{e}})\boldsymbol{r}_{\mathrm{t}} \tag{7}$$

The relative position kinematics and dynamics can be represented as[22]

$$\dot{\boldsymbol{r}}_{\mathrm{e}}=\boldsymbol{v}_{\mathrm{e}}-\boldsymbol{S}(\boldsymbol{\omega}_{\mathrm{s}})\boldsymbol{r}_{\mathrm{e}} \tag{8}$$

$$m\dot{\boldsymbol{v}}_{\mathrm{e}}=-m\boldsymbol{S}(\boldsymbol{\omega}_{\mathrm{s}})\boldsymbol{v}_{\mathrm{e}}+\boldsymbol{h}_{\mathrm{p}}+\boldsymbol{f}+\boldsymbol{f}_{\mathrm{d}} \tag{9}$$

where nonlinear term $\boldsymbol{h}_{\mathrm{p}}$ is

$$\boldsymbol{h}_{\mathrm{p}}=-\frac{m\mu(\boldsymbol{r}_{\mathrm{e}}+\boldsymbol{R}(\boldsymbol{\sigma}_{\mathrm{e}})\boldsymbol{r}_{\mathrm{t}})}{\left\|\boldsymbol{r}_{\mathrm{e}}+\boldsymbol{R}(\boldsymbol{\sigma}_{\mathrm{e}})\boldsymbol{r}_{\mathrm{t}}\right\|^{3}}-m\boldsymbol{R}(\boldsymbol{\sigma}_{\mathrm{e}})\ddot{\boldsymbol{r}}_{\mathrm{t}} \tag{10}$$

From Eqs.(8) and (9), we can see the relative translational dynamics has the item of the relative rotational dynamics. Therefore, the relative translational motion is coupled with rotational motion.

In order to facilitate the control system design process, the following assumptions and lemmas will be used in this paper.

Assumption 1 The disturbance vectors $\boldsymbol{f}_{\mathrm{d}}$ and $\boldsymbol{\tau}_{\mathrm{d}}$ are unknown but bounded with unknown bounds.

Assumption 2 The unknown mass m and inertial matrix $\boldsymbol{J}$ satisfies

$$\begin{cases} m_{\min}\leqslant m\leqslant m_{\max} \\ J_{ij,\min}\leqslant J_{ij}\leqslant J_{ij,\max} \quad i,j=1,2,3\end{cases} \tag{11}$$

Assumption 3 To satisfy the actuator saturation constraint, the real control inputs $\boldsymbol{f}$ and $\boldsymbol{\tau}$ are determined by the saturated function of commanded control force $\boldsymbol{f}_{\mathrm{c}}$ and control torque $\boldsymbol{\tau}_{\mathrm{c}}$, that is

$$f_i=\mathrm{sat}(f_{ci})=\begin{cases} f_{\max} & f_{ci}>f_{\max} \\ f_{ci} & -f_{\max}\leqslant f_{ci}\leqslant f_{\max} \\ -f_{\max} & f_{ci}\leqslant -f_{\max}\end{cases} \tag{12}$$

$$\tau_i=\mathrm{sat}(\tau_{ci})=\begin{cases} \tau_{\max} & \tau_{ci}>\tau_{\max} \\ \tau_{ci} & -\tau_{\max}\leqslant \tau_{ci}\leqslant \tau_{\max} \\ -\tau_{\max} & \tau_{ci}\leqslant -\tau_{\max}\end{cases} \tag{13}$$

Lemma 1 For arbitrary constant $\varepsilon>0$ and variable a, the following inequality always holds[23]

$$0\leqslant |a|-a\tanh\left(\frac{a}{\varepsilon}\right)\leqslant \varsigma\varepsilon,\varsigma=0.278\,5 \tag{14}$$

Lemma 2 Given any smooth function $\alpha(t)$, its derivative can be estimated by the following two-order command filter[24]

$$\hat{\dot{\alpha}}=\frac{\omega_{\mathrm{n}}^2 s}{s^2+2\zeta\omega_{\mathrm{n}}s+\omega_{\mathrm{n}}^2}\alpha \tag{15}$$

Choosing an appropriate damp ratio ζ and a sufficiently large natural frequency ω_{n} can ensure the accurate approximation[25].

The control objective of this paper is to design a control scheme based on the system formulated by Eqs.(1), (4), (8) and (9) without resorting to the exact knowledge of the mass and inertia parameters and despite the presence of external disturbance and actuator saturation such that:

(1) The relative position and attitude error achieve prescribed transient and steady-state performance.

(2) The ultimate boundedness of all closed-loop signals are guaranteed.

2 Controller Design

In this section, detailed design procedures via backstepping technique are presented to achieve the control objective.

2.1 Relative attitude controller design

The prescribed performance of relative attitude is achieved by ensuring that tracking error $\boldsymbol{\sigma}_{\mathrm{e}}$ evovles strictly within predefined bounds as follows

$$-\delta_{li}\rho_{\sigma i}\leqslant \sigma_{ei}(t)\leqslant \delta_{ui}\rho_{\sigma i}(t) \quad i=1,2,3 \tag{16}$$

where $0<\delta_{li},\delta_{ui}\leqslant 1$ are positive constants, $\rho_{\sigma i}(t)$ is the chosen prescribed performance function for attitude system. In this work, the exponentially decaying performance function are chosen as[26]

$$\rho_{\sigma i}(t)=(\rho_{\sigma i0}-\rho_{\sigma i\infty})\mathrm{e}^{-l_{\sigma i}t}+\rho_{\sigma i\infty} \tag{17}$$

where $\rho_{\sigma i0},\rho_{\sigma i\infty}$ and $l_{\sigma i}$ are strictly positive constants.

Denote

$$\bar{\sigma}_{ei}(t)=\frac{1}{\delta_i}\left(\frac{\sigma_{ei}(t)}{\rho_{\sigma i}(t)}-\frac{\delta_{ui}-\delta_{li}}{2}\right) \tag{18}$$

where $\delta_i=\left(\delta_{ui}+\delta_{li}\right)/2$. Based on Eqs. (16), (18), it implies

$$-1<\bar{\sigma}_{ei}(t)<1 \tag{19}$$

In order to transfer the prescribed performance control problem (19) to a normal unconstrained one, an error transformation is employed as

$$\bar{\sigma}_{ei}(t)=S(\chi_{\sigma_i}(t))=\frac{2}{\pi}\arctan(\chi_{\sigma_i}(t)) \tag{20}$$

Since $S(\chi_{\sigma i}(t))$ is strictly monotonic increasing, the inverse function of $S(\chi_{\sigma i}(t))$ exists. Then, the transformed error $\chi_{\sigma i}(t)$ can be expressed as

$$\chi_{\sigma i}(t)=S^{-1}(\bar{\sigma}_{ei}(t))=\tan\left(\frac{\pi}{2}\bar{\sigma}_{ei}(t)\right) \tag{21}$$

Invoking Eqs.(18) and (21), we have

$$\begin{cases}\lim\limits_{\chi_{\sigma i}\to+\infty}\sigma_{ei}(t)=\delta_{ui}\rho_{\sigma i}(t)\\ \lim\limits_{\chi_{\sigma i}\to-\infty}\sigma_{ei}(t)=-\delta_{li}\rho_{\sigma i}(t)\end{cases} \tag{22}$$

From Eq.(21), we can obtain

$$\dot{\chi}_{\sigma i}=\frac{\pi}{2\delta_i\rho_{\sigma i}}\left[1+\tan^2\left(\frac{\pi}{2}\bar{\sigma}_{ei}\right)\right]\cdot\left(\dot{\sigma}_{ei}-\frac{\sigma_{ei}\dot{\rho}_{\sigma i}}{\rho_{\sigma i}}\right) \tag{23}$$

Denote

$$\boldsymbol{R}_\sigma=\mathrm{diag}\left\{r_{\sigma1},r_{\sigma2},r_{\sigma3}\right\},\boldsymbol{\upsilon}_\sigma=[\upsilon_{\sigma1},\upsilon_{\sigma2},\upsilon_{\sigma3}]^{\mathrm{T}} \tag{24}$$

where $r_{\sigma i}=\frac{\pi}{2\delta_i\rho_{\sigma i}}\left[1+\tan^2\left(\frac{\pi}{2}\bar{\sigma}_{ei}\right)\right],\upsilon_{\sigma i}=-\frac{\sigma_{ei}\dot{\rho}_{\sigma i}}{\rho_{\sigma i}}$.

Then from Eqs.(1), Eq.(23) can be written in compact form as

$$\dot{\boldsymbol{\chi}}_\sigma=\boldsymbol{R}_\sigma(\boldsymbol{G}(\boldsymbol{\sigma}_e)\boldsymbol{\omega}_e+\boldsymbol{\upsilon}_\sigma) \tag{25}$$

Then, the problem of achieving prescribed performance of relative attitude error has been converted into designing a control scheme to ensure the boundedness of the transformed error $\boldsymbol{\sigma}_e$. In what follows, the following coordinate changes are firstly employed

$$\boldsymbol{x}_1=\boldsymbol{\chi}_\sigma-\boldsymbol{\xi}_{\sigma1} \tag{26}$$

$$\boldsymbol{x}_2=\boldsymbol{\omega}_e-\boldsymbol{\alpha}_\sigma-\boldsymbol{\xi}_{\sigma2} \tag{27}$$

where $\boldsymbol{\alpha}_\sigma$ is the virtual control signal to be designed latter; $\boldsymbol{\xi}_{\sigma1}$ the compensation term satisfying

$$\dot{\boldsymbol{\xi}}_{\sigma1}=-\boldsymbol{K}_{\sigma1}\boldsymbol{\xi}_{\sigma1}+\boldsymbol{K}_{\sigma21}\boldsymbol{\xi}_{\sigma2} \tag{28}$$

where $\boldsymbol{K}_{\sigma1}$ and $\boldsymbol{K}_{\sigma21}$ are positive matrixes. The new signal $\boldsymbol{\xi}_{\sigma2}$ is introduced to deal with the saturation effect through following novel auxiliary system

$$\hat{\boldsymbol{J}}\dot{\boldsymbol{\xi}}_{\sigma2}=-\boldsymbol{K}_{\sigma2}\frac{e^{\boldsymbol{\xi}_{\sigma2}}-1}{e^{\boldsymbol{\xi}_{\sigma2}}+1}+\Delta\boldsymbol{\tau} \tag{29}$$

where $\boldsymbol{K}_{\sigma2}$ is a positive matrix, $\hat{\boldsymbol{J}}$ the estimate of $\boldsymbol{J}$, $\Delta\boldsymbol{\tau}=\boldsymbol{\tau}-\boldsymbol{\tau}_c$ the difference between commanded and actual control torque.

Considering Eqs. (26), (27) and (28), the time derivative of $\boldsymbol{x}_1$ can be expressed as

$$\dot{\boldsymbol{x}}_1=\boldsymbol{R}_\sigma\boldsymbol{G}(\boldsymbol{x}_2+\boldsymbol{\alpha}_\sigma+\boldsymbol{\xi}_{\sigma2})+\boldsymbol{R}_\sigma\boldsymbol{\upsilon}_\sigma+\boldsymbol{K}_{\sigma1}\boldsymbol{\xi}_{\sigma1}-\boldsymbol{K}_{\sigma21}\boldsymbol{\xi}_{\sigma2} \tag{30}$$

The virtual control law $\boldsymbol{\alpha}_\sigma$ is designed as

$$\begin{aligned}\boldsymbol{\alpha}_\sigma=&-\boldsymbol{\xi}_{\sigma2}-\boldsymbol{G}^{-1}\boldsymbol{\upsilon}_\sigma-\boldsymbol{G}^{-1}\boldsymbol{R}_\sigma^{-1}\boldsymbol{K}_1\boldsymbol{x}_1-\\&\boldsymbol{G}^{-1}\boldsymbol{R}_\sigma^{-1}(\boldsymbol{K}_{\sigma1}\boldsymbol{\xi}_{\sigma1}-\boldsymbol{K}_{\sigma21}\boldsymbol{\xi}_{\sigma2})\end{aligned} \tag{31}$$

where $\boldsymbol{K}_1$ is a positive matrix. Choosing the following Lyapunov function candidate

$$V_1=\frac{1}{2}\boldsymbol{x}_1^{\mathrm{T}}\boldsymbol{x}_1+\frac{1}{2}\boldsymbol{\xi}_{\sigma1}^{\mathrm{T}}\boldsymbol{\xi}_{\sigma1} \tag{32}$$

Considering Eqs. (28), (30) and (31), the time derivative of V_1 is given by

$$\dot{V}_1=\boldsymbol{x}_1^{\mathrm{T}}\boldsymbol{R}_\sigma\boldsymbol{G}\boldsymbol{x}_2-\boldsymbol{x}_1^{\mathrm{T}}\boldsymbol{K}_1\boldsymbol{x}_1-\boldsymbol{\xi}_{\sigma1}^{\mathrm{T}}\boldsymbol{K}_{\sigma1}\boldsymbol{\xi}_{\sigma1}+\boldsymbol{\xi}_{\sigma1}^{\mathrm{T}}\boldsymbol{K}_{\sigma21}\boldsymbol{\xi}_{\sigma2} \tag{33}$$

To overcome the explosion of complexity caused in backstepping design, introducing a new variable $\hat{\alpha}_\sigma$ as the output of a command filter (15), and passing the virtual control (31) through it produces

$$\dot{\boldsymbol{\alpha}}_\sigma=\dot{\hat{\boldsymbol{\alpha}}}_\sigma+\Delta\dot{\boldsymbol{\alpha}}_\sigma \tag{34}$$

where $\Delta\dot{\boldsymbol{\alpha}}_\sigma$ denotes the estimate error.

Taking the derivative of Eq.(27), then from Eqs.(4) and (34), we have

$$\begin{aligned}\boldsymbol{J}\dot{\boldsymbol{x}}_2=&\boldsymbol{C}_a\boldsymbol{x}_2+\boldsymbol{C}_a(\boldsymbol{\alpha}_\sigma+\boldsymbol{\xi}_{\sigma2})+\boldsymbol{h}_a+\boldsymbol{\tau}+\boldsymbol{\tau}_d-\boldsymbol{J}\dot{\hat{\boldsymbol{\alpha}}}_\sigma-\\&\boldsymbol{J}\Delta\dot{\boldsymbol{\alpha}}_\sigma-\boldsymbol{J}\dot{\boldsymbol{\xi}}_{\sigma2}\end{aligned} \tag{35}$$

From Assumption 2, a linear operator $\boldsymbol{L}(\cdot)$: $\mathbf{R}^3\to\mathbf{R}^{3\times6}$ acting on an arbitrary vector $\boldsymbol{a}=[a_1\quad a_2\quad a_3]^{\mathrm{T}}$ is introduced to isolate the unknown inertia matrix $\boldsymbol{J}$ such that

$$\boldsymbol{J}\boldsymbol{a}=\boldsymbol{L}(\boldsymbol{a})\boldsymbol{\theta}_J \tag{36}$$

where

$$\boldsymbol{L}(\boldsymbol{a})=\begin{bmatrix}a_1&0&0&a_2&a_3&0\\0&a_2&0&a_1&0&a_3\\0&0&a_3&0&a_1&a_2\end{bmatrix} \tag{37}$$

and

$$\boldsymbol{\theta}_J=\left[J_{11},J_{22},J_{33},J_{12},J_{13},J_{23}\right]^{\mathrm{T}} \tag{38}$$

From Eq.(36), we know

$$\begin{cases}\boldsymbol{h}_a=\boldsymbol{H}_{\sigma1}\boldsymbol{\theta}_J,\boldsymbol{J}\dot{\hat{\boldsymbol{\alpha}}}_\sigma=\boldsymbol{H}_{\sigma2}\boldsymbol{\theta}_J\\ \boldsymbol{C}_a(\boldsymbol{\alpha}_\sigma+\boldsymbol{\xi}_{\sigma2})=\boldsymbol{H}_{\sigma3}\boldsymbol{\theta}_J\end{cases} \tag{39}$$

where

$$\begin{cases}\boldsymbol{H}_{\sigma1}=-\boldsymbol{S}(\boldsymbol{R}(\boldsymbol{\sigma}_e)\boldsymbol{\omega}_t)\boldsymbol{L}(\boldsymbol{R}(\boldsymbol{\sigma}_e)\boldsymbol{\omega}_t)-\\ \qquad\boldsymbol{L}(\boldsymbol{R}(\boldsymbol{\sigma}_e)\boldsymbol{\omega}_t)\\ \boldsymbol{H}_{\sigma2}=\boldsymbol{L}(\dot{\hat{\boldsymbol{\alpha}}}_\sigma)\\ \boldsymbol{H}_{\sigma3}=-\boldsymbol{S}(\boldsymbol{\alpha}_\sigma+\boldsymbol{\xi}_{\sigma2})\boldsymbol{L}(\boldsymbol{\omega}_e+\boldsymbol{R}(\boldsymbol{\sigma}_e)\boldsymbol{\omega}_t)-\\ \qquad\boldsymbol{S}(\boldsymbol{R}(\boldsymbol{\sigma}_e)\boldsymbol{\omega}_t)\boldsymbol{L}(\boldsymbol{\alpha}_\sigma+\boldsymbol{\xi}_{\sigma2})-\\ \qquad\boldsymbol{L}(\boldsymbol{S}(\boldsymbol{R}(\boldsymbol{\sigma}_e)\boldsymbol{\omega}_t)(\boldsymbol{\alpha}_\sigma+\boldsymbol{\xi}_{\sigma2}))\end{cases} \tag{40}$$

In view of Eqs.(13), (34) and (39), Eq.(35) can be rewritten as

$$\boldsymbol{J}\dot{\boldsymbol{x}}_2=\boldsymbol{C}_a\boldsymbol{x}_2+\boldsymbol{H}_{\sigma1}\boldsymbol{\theta}_J+\bar{\boldsymbol{\tau}}_d+\boldsymbol{\tau}_c+\Delta\boldsymbol{\tau}-\hat{\boldsymbol{J}}\dot{\boldsymbol{\xi}}_{\sigma2}+\boldsymbol{H}_{\sigma4}\tilde{\boldsymbol{\theta}}_J \tag{41}$$

where $\boldsymbol{H}_{\sigma4}=L(\dot{\boldsymbol{\xi}}_{\sigma2})$, $\boldsymbol{H}_{\sigma}=\boldsymbol{H}_{\sigma1}-\boldsymbol{H}_{\sigma2}+\boldsymbol{H}_{\sigma3}$, $\tilde{\boldsymbol{\theta}}_J=\hat{\boldsymbol{\theta}}_J-\boldsymbol{\theta}_J$ is the estimate error of $\boldsymbol{\theta}_J$ and $\bar{\boldsymbol{\tau}}_{\rm d}=\boldsymbol{\tau}_{\rm d}-\boldsymbol{J}\Delta\dot{\boldsymbol{\alpha}}_{\sigma}$ is the lumped uncertainty.

According to Assumption 1 and Lemma 2, $\bar{\boldsymbol{\tau}}_{\rm d}$ is bounded, namely, $\left|\bar{\tau}_{{\rm d}i}\right|\leqslant\eta_{\sigma i}(i=1,2,3)$. Then, we can design the relative attitude control input $\boldsymbol{\tau}_{\rm c}$ as

$$\boldsymbol{\tau}_{\rm c}=-\boldsymbol{G}^{\rm T}\boldsymbol{R}_{\sigma}^{\rm T}\boldsymbol{x}_1-\boldsymbol{K}_2\boldsymbol{x}_2-\boldsymbol{K}_{\sigma2}\frac{{\rm e}^{\boldsymbol{\xi}_{\sigma2}}-1}{{\rm e}^{\boldsymbol{\xi}_{\sigma2}}+1}-\boldsymbol{H}_{\sigma}\hat{\boldsymbol{\theta}}_J-\tanh\left(\frac{\boldsymbol{x}_2}{\varepsilon}\right)\hat{\boldsymbol{\eta}}_{\sigma}-\frac{(1+k_{\sigma})\boldsymbol{x}_2}{\left\|\boldsymbol{x}_2\right\|^2+b_{\sigma2}}\left|\boldsymbol{\xi}_{\sigma1}^{\rm T}\boldsymbol{K}_{\sigma21}\boldsymbol{\xi}_{\sigma2}\right| \tag{42}$$

where $\boldsymbol{K}_2=\boldsymbol{K}_2^{\rm T}$ is a symmetric matrix. Design adaptation laws for $\hat{\boldsymbol{\theta}}_J$ and $\hat{\boldsymbol{\eta}}_{\sigma}$ as

$$\begin{cases}\dot{\hat{\theta}}_J=\operatorname{Proj}(\boldsymbol{\Gamma}_1\bar{\boldsymbol{H}}_{\sigma}^{\rm T}\boldsymbol{x}_2)\\ \dot{\hat{\eta}}_{\sigma}=\boldsymbol{\Gamma}_2\left(\tanh\left(\frac{\boldsymbol{x}_2}{\varepsilon}\right)\boldsymbol{x}_2-k_{\sigma}\hat{\boldsymbol{\eta}}_{\sigma}\right)\end{cases} \tag{43}$$

where the Proj$(\cdot)$ is a Lipschitz continuous projection algorithm[27], $\bar{\boldsymbol{H}}_{\sigma}=\boldsymbol{H}_{\sigma}-\boldsymbol{H}_{\sigma4}$, $\boldsymbol{\Gamma}_1$ and $\boldsymbol{\Gamma}_2$ are positive define matrixes. Moreover, the notation $\tanh(\cdot)$ is defined as

$$\tanh\left(\frac{\boldsymbol{x}_2}{\varepsilon}\right)=\operatorname{diag}\left\{\tanh\left(\frac{x_{2i}}{\varepsilon}\right)\right\}\quad i=1,2,3 \tag{44}$$

Define the estimate error of $\boldsymbol{\eta}_{\sigma}$ as $\tilde{\boldsymbol{\eta}}_{\sigma}=\hat{\boldsymbol{\eta}}_{\sigma}-\boldsymbol{\eta}_{\sigma}$, then a Lyapunov function is constructed as

$$V_2=V_1+\frac{1}{2}\boldsymbol{x}_2^{\rm T}\boldsymbol{J}\boldsymbol{x}_2+\frac{1}{2}\tilde{\boldsymbol{\theta}}_J^{\rm T}\boldsymbol{\Gamma}_1^{-1}\tilde{\boldsymbol{\theta}}_J+\frac{1}{2}\tilde{\boldsymbol{\eta}}_{\sigma}^{\rm T}\boldsymbol{\Gamma}_2^{-1}\tilde{\boldsymbol{\eta}}_{\sigma}+\frac{1}{2b_{\sigma}}k_{\sigma}^2 \tag{45}$$

where k_{σ} is the auxiliary variable[28] satisfying

$$\dot{k}_{\sigma}=\begin{cases}\dfrac{b_{\sigma}}{k_{\sigma}}\dfrac{k_{\sigma}\left\|\boldsymbol{x}_2\right\|^2-b_{\sigma1}}{\left\|\boldsymbol{x}_2\right\|^2+b_{\sigma2}}\left|\boldsymbol{\xi}_{\sigma1}^{\rm T}\boldsymbol{K}_{\sigma21}\boldsymbol{\xi}_{\sigma2}\right| & k_{\sigma}\neq0\\ b_{\sigma2} & k_{\sigma}=0\end{cases} \tag{46}$$

The derivative of Eq.(45) can be derived as

$$\dot{V}_2=\dot{V}_1+\boldsymbol{x}_2^{\rm T}\boldsymbol{J}\dot{\boldsymbol{x}}_2+\tilde{\boldsymbol{\theta}}_J^{\rm T}\boldsymbol{\Gamma}_1^{-1}\dot{\hat{\theta}}_J+\tilde{\boldsymbol{\eta}}_{\sigma}^{\rm T}\boldsymbol{\Gamma}_2^{-1}\dot{\hat{\eta}}_{\sigma}+\frac{1}{b_{\sigma}}k_{\sigma}\dot{k}_{\sigma} \tag{47}$$

Substituting Eqs.(33), (41), and Eq.(42) into (47) and considering $\boldsymbol{x}_2^{\rm T}\boldsymbol{C}_a\boldsymbol{x}_2=0$ yields

$$\dot{V}_2=-\boldsymbol{x}_1^{\rm T}\boldsymbol{K}_1\boldsymbol{x}_1-\boldsymbol{x}_2^{\rm T}\boldsymbol{K}_2\boldsymbol{x}_2-\boldsymbol{\xi}_{\sigma1}^{\rm T}\boldsymbol{K}_{\sigma1}\boldsymbol{\xi}_{\sigma1}+\tilde{\boldsymbol{\theta}}_J^{\rm T}\boldsymbol{\Gamma}_1^{-1}\dot{\hat{\theta}}_J-\boldsymbol{x}_2^{\rm T}\bar{\boldsymbol{H}}_{\sigma}\tilde{\boldsymbol{\theta}}_J+\tilde{\boldsymbol{\eta}}_{\sigma}^{\rm T}\boldsymbol{\Gamma}_2^{-1}\dot{\hat{\eta}}_{\sigma}+\boldsymbol{x}_2^{\rm T}\bar{\boldsymbol{\tau}}_{\rm d}-\boldsymbol{x}_2^{\rm T}\operatorname{Tanh}\left(\frac{\boldsymbol{x}_2}{\varepsilon}\right)\hat{\boldsymbol{\eta}}_{\sigma}+\boldsymbol{\xi}_{\sigma1}^{\rm T}\boldsymbol{K}_{\sigma21}\boldsymbol{\xi}_{\sigma2}-\frac{(1+k_{\sigma})\boldsymbol{x}_2}{\left\|\boldsymbol{x}_2\right\|^2+b_{\sigma2}}\left|\boldsymbol{\xi}_{\sigma1}^{\rm T}\boldsymbol{K}_{\sigma21}\boldsymbol{\xi}_{\sigma2}\right|+\frac{1}{b_{\sigma}}k_{\sigma}\dot{k}_{\sigma} \tag{48}$$

According to Lemma 1, we have

$$\boldsymbol{x}_2^{\rm T}\bar{\boldsymbol{\tau}}_{\rm d}\leqslant\boldsymbol{x}_2^{\rm T}\tanh\left(\frac{\boldsymbol{x}_2}{\varepsilon}\right)\boldsymbol{\eta}_{\sigma}+\frac{\left\|\boldsymbol{\varphi}_{\sigma}\right\|^2}{2}+\frac{\left\|\boldsymbol{\eta}_{\sigma}\right\|^2}{2} \tag{49}$$

where $\boldsymbol{\varphi}_{\sigma}=[\varsigma\varepsilon,\varsigma\varepsilon,\varsigma\varepsilon]^{\rm T}$.

Applying to the property of projection operator, the following inequality holds

$$\tilde{\boldsymbol{\theta}}_J^{\rm T}\boldsymbol{\Gamma}_1^{-1}\dot{\hat{\theta}}_J-\boldsymbol{x}_2^{\rm T}\bar{\boldsymbol{H}}_{\sigma}\tilde{\boldsymbol{\theta}}_J\leqslant0 \tag{50}$$

In virtue of Eqs.(49) and (50), substituting Eqs.(43) and (46) into Eq.(48), we have

$$\dot{V}_2=-\boldsymbol{x}_1^{\rm T}\boldsymbol{K}_1\boldsymbol{x}_1-\boldsymbol{x}_2^{\rm T}\boldsymbol{K}_2\boldsymbol{x}_2-\boldsymbol{\xi}_{\sigma1}^{\rm T}\boldsymbol{K}_{\sigma1}\boldsymbol{\xi}_{\sigma1}-k_{\sigma}\tilde{\boldsymbol{\eta}}_{\sigma}^{\rm T}\hat{\boldsymbol{\eta}}_{\sigma}+\frac{\left\|\boldsymbol{\varphi}_{\sigma}\right\|^2}{2}+\frac{\left\|\boldsymbol{\eta}_{\sigma}\right\|^2}{2} \tag{51}$$

From Schwartz inequality, the following inequality can be obtained

$$-k_{\sigma}\tilde{\boldsymbol{\eta}}_{\sigma}^{\rm T}\hat{\boldsymbol{\eta}}_{\sigma}\leqslant-\frac{k_{\sigma}}{2}\left\|\tilde{\boldsymbol{\eta}}_{\sigma}\right\|^2+\frac{k_{\sigma}}{2}\left\|\boldsymbol{\eta}_{\sigma}\right\|^2 \tag{52}$$

Hence, substituting Eq.(52) into Eq.(51), one has the following inequality

$$\dot{V}_2=-\boldsymbol{x}_1^{\rm T}\boldsymbol{K}_1\boldsymbol{x}_1-\boldsymbol{x}_2^{\rm T}\boldsymbol{K}_2\boldsymbol{x}_2-\boldsymbol{\xi}_{\sigma1}^{\rm T}\boldsymbol{K}_{\sigma1}\boldsymbol{\xi}_{\sigma1}-\frac{k_{\sigma}}{2}\left\|\tilde{\boldsymbol{\eta}}_{\sigma}\right\|^2+\psi_{\sigma} \tag{53}$$

where $\psi_{\sigma}=\frac{k_{\sigma}}{2}\left\|\boldsymbol{\eta}_{\sigma}\right\|^2+\frac{\left\|\boldsymbol{\varphi}_{\sigma}\right\|^2}{2}+\frac{\left\|\boldsymbol{\eta}_{\sigma}\right\|^2}{2}$.

From Eq.(53), the stabilization of the transformed relative attitude systems (4) and (25) is ensured, then the relative attitude error can be guaranteed within prescribed performance bounds in Eq.(16). The main result is summarized in the following theorem.

Theorem 1 Consider the relative attitude dynamic systems (1) and (4) under the control torque constraint (13) with Assumptions 1—3, the proposed controller (42), adaptation laws (43) and (46) can guarantee that all signals in the closed-loop system are uniformly ultimately bounded, and the relative attitude error remains within the prescribed performance bounds all the time.

2.2 Relative position controller design

The prescribed performance of relative position is achieved by ensuring that tracking error $\boldsymbol{r}_{\rm e}$ evolves strictly within predefined bounds as follows:

$$-\delta_{li}\rho_{pi} \leqslant r_{ei}(t) \leqslant \delta_{ui}\rho_{pi}(t) \quad i=1,2,3 \tag{54}$$

where the exponentially decaying performance function $\rho_{pi}(t)$ are chosen as[26]

$$\rho_{pi}(t)=(\rho_{pi0}-\rho_{pi\infty})\mathrm{e}^{-l_{pi}t}+\rho_{pi} \tag{55}$$

where ρ_{pi0}, $\rho_{pi\infty}$ and l_{pi} are strictly positive constants.

Denote

$$\bar{r}_{ei}(t)=\frac{1}{\delta_i}\left(\frac{r_{ei}(t)}{\rho_{pi}(t)}-\frac{\delta_{ui}-\delta_{li}}{2}\right) \tag{56}$$

where $\delta_i=(\delta_{ui}+\delta_{li})/2$. Based on Eqs. (54) and (56), it implies

$$-1<\bar{r}_{ei}(t)<1 \tag{57}$$

In order to transfer the prescribed performance control problem (57) to a normal unconstrained one, an error transformation is employed as

$$\bar{r}_{ei}(t)=S(\chi_{p_i}(t))=\frac{2}{\pi}\arctan(\chi_{p_i}(t)) \tag{58}$$

Since $S(\chi_{pi}(t))$ is strictly monotonic increasing, the inverse function of $S(\chi_{pi}(t))$ exists. Then, the transformed error $\chi_{pi}(t)$ can be expressed as

$$\chi_{pi}(t)=S^{-1}(\bar{r}_{ei}(t))=\tan\left(\frac{\pi}{2}\bar{r}_{ei}(t)\right) \tag{59}$$

Invoking Eqs.(56) and (59), we have

$$\begin{cases}\lim\limits_{\chi_{pi}\to+\infty} r_{ei}(t)=\delta_{ui}\rho_{pi}(t)\\ \lim\limits_{\chi_{pi}\to-\infty} r_{ei}(t)=-\delta_{li}\rho_{pi}(t)\end{cases} \tag{60}$$

From Eq.(59), we can obtain

$$\dot{\chi}_{pi}=\frac{\pi}{2\delta_i\rho_{pi}}\left[1+\tan^2\left(\frac{\pi}{2}\bar{r}_{ei}\right)\right]\cdot\left(\dot{r}_{ei}-\frac{r_{ei}\dot{\rho}_{pi}}{\rho_{pi}}\right) \tag{61}$$

Denote

$$\boldsymbol{R}_p=\mathrm{diag}\{r_{p1},r_{p2},r_{p3}\},\boldsymbol{\upsilon}_p=[\upsilon_{p1},\upsilon_{p2},\upsilon_{p3}]^{\mathrm{T}} \tag{62}$$

where $r_{pi}=\dfrac{\pi}{2\delta_i\rho_{pi}}\left[1+\tan^2\left(\dfrac{\pi}{2}\bar{r}_{ei}\right)\right]$, $\upsilon_{\sigma i}=-\dfrac{r_{ei}\dot{\rho}_{pi}}{\rho_{pi}}$.

Then from Eq.(8), Eq.(61) can be written in compact form as

$$\dot{\boldsymbol{\chi}}_p=\boldsymbol{R}_p(\boldsymbol{v}_e-\boldsymbol{S}(\boldsymbol{\omega}_s)\boldsymbol{r}_e+\boldsymbol{\upsilon}_p) \tag{63}$$

Then, the problem of achieving prescribed performance of relative position error has been converted into designing a control scheme to ensure the boundedness of the transformed error $\boldsymbol{r}_e$.

Define the following coordinate changes

$$\boldsymbol{y}_1=\boldsymbol{\chi}_p-\boldsymbol{\xi}_{p1} \tag{64}$$

$$\boldsymbol{y}_2=\boldsymbol{v}_e-\boldsymbol{\alpha}_p-\boldsymbol{\xi}_{p2} \tag{65}$$

where $\boldsymbol{\alpha}_p$ is the virtual control signal to be designed laer; $\boldsymbol{\xi}_{\sigma1}$ is the compensation term satisfying

$$\dot{\boldsymbol{\xi}}_{p1}=-\boldsymbol{K}_{p1}\boldsymbol{\xi}_{p1}+\boldsymbol{K}_{p21}\boldsymbol{\xi}_{p2} \tag{66}$$

where $\boldsymbol{K}_{p1}$ and $\boldsymbol{K}_{p21}$ are positive matrixes; The new signal $\boldsymbol{\xi}_{p2}$ is introduced to deal with the saturation effect through following novel auxiliary system

$$\hat{m}\dot{\boldsymbol{\xi}}_{p2}=-\boldsymbol{K}_{p2}\frac{\mathrm{e}^{\boldsymbol{\xi}_{p2}}-1}{\mathrm{e}^{\boldsymbol{\xi}_{p2}}+1}+\Delta\boldsymbol{f} \tag{67}$$

where $\boldsymbol{K}_{p2}$ is a positive matrix, $\hat{m}$ the estimate of m, $\Delta\boldsymbol{f}=\boldsymbol{f}-\boldsymbol{f}_c$ denotes the difference between commanded and actual control force.

Considering Eqs. (64), (65) and (66), the time derivative of $\boldsymbol{y}_1$ can be expressed as

$$\dot{\boldsymbol{y}}_1=\boldsymbol{R}_p(\boldsymbol{y}_2+\boldsymbol{\alpha}_p+\boldsymbol{\xi}_{p2}-\boldsymbol{S}(\boldsymbol{\omega}_s)\boldsymbol{r}_e+\boldsymbol{\upsilon}_p)+\boldsymbol{K}_{p1}\boldsymbol{\xi}_{p1}-\boldsymbol{K}_{p21}\boldsymbol{\xi}_{p2} \tag{68}$$

The virtual control law $\boldsymbol{\alpha}_p$ is designed as

$$\boldsymbol{\alpha}_p=-\boldsymbol{R}_p^{-1}(\boldsymbol{K}_{p1}\boldsymbol{\xi}_{p1}-\boldsymbol{K}_{p21}\boldsymbol{\xi}_{p2}+\boldsymbol{K}_3\boldsymbol{y}_1)+\boldsymbol{S}(\boldsymbol{\omega}_s)\boldsymbol{r}_e-\boldsymbol{\upsilon}_p-\boldsymbol{\xi}_{p2} \tag{69}$$

where $\boldsymbol{K}_3$ is a positive matrix. Choosing the following Lyapunov function candidate

$$V_3=\frac{1}{2}\boldsymbol{y}_1^{\mathrm{T}}\boldsymbol{y}_1+\frac{1}{2}\boldsymbol{\xi}_{p1}^{\mathrm{T}}\boldsymbol{\xi}_{p1} \tag{70}$$

Considering Eqs. (66), (68) and (69), the time derivative of V_3 is given by

$$\dot{V}_3=\boldsymbol{y}_1^{\mathrm{T}}\boldsymbol{R}_p\boldsymbol{y}_2-\boldsymbol{y}_1^{\mathrm{T}}\boldsymbol{K}_3\boldsymbol{y}_1-\boldsymbol{\xi}_{p1}^{\mathrm{T}}\boldsymbol{K}_{p1}\boldsymbol{\xi}_{p1}+\boldsymbol{\xi}_{p1}^{\mathrm{T}}\boldsymbol{K}_{p21}\boldsymbol{\xi}_{p2} \tag{71}$$

To overcome the explosion of complexity caused in backstepping design, introducing a new variable $\hat{\alpha}_p$ as the output of a command filter (15), and passing the virtual control (69) through it produces

$$\dot{\boldsymbol{\alpha}}_p=\hat{\dot{\alpha}}_p+\Delta\dot{\boldsymbol{\alpha}}_p \tag{72}$$

where $\Delta\dot{\boldsymbol{\alpha}}_p$ denotes the estimate error.

Taking the derivative of Eq.(65), then from Eqs.(9) and (72), we have

$$m\dot{\boldsymbol{y}}_2=-m\boldsymbol{S}(\boldsymbol{\omega}_s)\boldsymbol{y}_2-m\boldsymbol{S}(\boldsymbol{\omega}_s)(\boldsymbol{\alpha}_p+\boldsymbol{\xi}_{p2})+\boldsymbol{h}_p+\boldsymbol{f}+\boldsymbol{f}_d-m\hat{\dot{\alpha}}_p-m\Delta\dot{\boldsymbol{\alpha}}_p-m\dot{\boldsymbol{\xi}}_{p2} \tag{73}$$

From Assumption 2, following relations is introduced to isolate the unknown mass m such that

$$\begin{cases}\boldsymbol{h}_p=m\boldsymbol{\vartheta}_{p1},\ -m\hat{\dot{\alpha}}_p=m\boldsymbol{\vartheta}_{p2}\\ -m\boldsymbol{S}(\boldsymbol{\omega}_s)(\boldsymbol{\alpha}_p+\boldsymbol{\xi}_{p2})=m\boldsymbol{\vartheta}_{p3}\end{cases} \tag{74}$$

where

$$\begin{cases}\boldsymbol{\vartheta}_{p2}=-\hat{\dot{\alpha}}_p\\ \boldsymbol{\vartheta}_{p1}=-\dfrac{\mu(\boldsymbol{r}_e+\boldsymbol{R}(\boldsymbol{\sigma}_e)\boldsymbol{r}_t)}{\left\|\boldsymbol{r}_e+\boldsymbol{R}(\boldsymbol{\sigma}_e)\boldsymbol{r}_t\right\|^3}-\boldsymbol{R}(\boldsymbol{\sigma}_e)\ddot{\boldsymbol{r}}_t\\ \boldsymbol{\vartheta}_{p3}=-\boldsymbol{S}(\boldsymbol{\omega}_s)(\boldsymbol{\alpha}_p+\boldsymbol{\xi}_{p2})\end{cases} \tag{75}$$

In view of Eqs.(12), (72) and (74), Eq.(73) can be rewritten as

$$m\dot{\boldsymbol{y}}_2=-m\boldsymbol{S}(\boldsymbol{\omega}_s)\boldsymbol{y}_2+m\boldsymbol{\vartheta}_p+\bar{\boldsymbol{f}}_d+\boldsymbol{f}_c-\hat{m}\dot{\boldsymbol{\xi}}_{p2}+\tilde{m}\boldsymbol{\vartheta}_{p4} \tag{76}$$

where $\boldsymbol{\vartheta}_{p4}=\dot{\boldsymbol{\xi}}_{p2}$, $\boldsymbol{\vartheta}_p=\boldsymbol{\vartheta}_{p1}+\boldsymbol{\vartheta}_{p2}+\boldsymbol{\vartheta}_{p3}$, $\tilde{m}=\hat{m}-m$ is the estimate error of m and $\bar{\boldsymbol{f}}_d=\boldsymbol{f}_d-m\Delta\dot{\boldsymbol{\alpha}}_p$ is the lumped uncertainty.

According to Assumption 1 and Lemma 2, $\bar{\boldsymbol{f}}_d$ is bounded, namely, $\left|\bar{f}_{di}\right|\leqslant\eta_{pi}(i=1,2,3)$. Then, we can design the relative position control input $\boldsymbol{f}_c$ as

$$\boldsymbol{f}_c=-\boldsymbol{R}_p^{T}\boldsymbol{y}_1-\boldsymbol{K}_4\boldsymbol{y}_2-\boldsymbol{K}_{p2}\boldsymbol{\xi}_{p2}-\hat{m}\boldsymbol{\vartheta}_p-\tanh\left(\frac{\boldsymbol{y}_2}{\varepsilon}\right)\hat{\boldsymbol{\eta}}_p-\frac{(1+k_p)\boldsymbol{y}_2}{\left\|\boldsymbol{y}_2\right\|^2+b_{p2}}\left|\boldsymbol{\xi}_{p1}^{T}\boldsymbol{K}_{p21}\boldsymbol{\xi}_{p2}\right| \tag{77}$$

where $\boldsymbol{K}_4=\boldsymbol{K}_4^{T}$ is a symmetric matrix. Design adaptation laws for $\hat{m}$ and $\hat{\boldsymbol{\eta}}_p$ as

$$\begin{cases}\dot{\hat{m}}=\operatorname{Proj}(\gamma_3\bar{\boldsymbol{\vartheta}}_p^{T}\boldsymbol{y}_2)\\ \dot{\hat{\boldsymbol{\eta}}}_p=\boldsymbol{\Gamma}_4\left(\tanh\left(\dfrac{\boldsymbol{y}_2}{\varepsilon}\right)\boldsymbol{y}_2-k_p\hat{\boldsymbol{\eta}}_p\right)\end{cases} \tag{78}$$

where $\bar{\boldsymbol{\vartheta}}_p=\boldsymbol{\vartheta}_p-\boldsymbol{\vartheta}_{p4}$, γ_3 is a positive constant and $\boldsymbol{\Gamma}_4$ is a define matrix.

Define the estimate error of $\boldsymbol{\eta}_p$ as $\tilde{\boldsymbol{\eta}}_p=\hat{\boldsymbol{\eta}}_p-\boldsymbol{\eta}_p$, then a Lyapunov function is constructed as

$$V_4=V_3+\frac{1}{2}m\boldsymbol{y}_2^{T}\boldsymbol{y}_2+\frac{1}{2\gamma_3}\tilde{m}^2+\frac{1}{2}\tilde{\boldsymbol{\eta}}_p^{T}\boldsymbol{\Gamma}_4^{-1}\tilde{\boldsymbol{\eta}}_p+\frac{1}{2b_p}k_p^2 \tag{79}$$

where k_p is the auxiliary variable[28] satisfying

$$\dot{k}_p=\begin{cases}\dfrac{b_p}{k_p}\dfrac{k_p\left\|\boldsymbol{y}_2\right\|^2-b_{p1}}{\left\|\boldsymbol{y}_2\right\|^2+b_{p2}}\left|\boldsymbol{\xi}_{p1}^{T}\boldsymbol{K}_{p21}\boldsymbol{\xi}_{p2}\right| & k_p\neq 0\\ b_{p2} & k_p=0\end{cases} \tag{80}$$

The derivative of Eq.(79) can be derived as

$$\dot{V}_4=\dot{V}_3+m\boldsymbol{y}_2^{T}\dot{\boldsymbol{y}}_2+\frac{1}{\gamma_3}\tilde{m}\dot{\hat{m}}+\tilde{\boldsymbol{\eta}}_p^{T}\boldsymbol{\Gamma}_4^{-1}\dot{\hat{\eta}}_p+\frac{1}{b_p}k_p\dot{k}_p \tag{81}$$

Substituting Eqs.(71), (76), and (77) into Eq.(81) and considering $\boldsymbol{y}_2^{T}\boldsymbol{S}(\boldsymbol{\omega}_s)\boldsymbol{y}_2=0$ yields

$$\dot{V}_4=-\boldsymbol{y}_1^{T}\boldsymbol{K}_3\boldsymbol{y}_1-\boldsymbol{y}_2^{T}\boldsymbol{K}_4\boldsymbol{y}_2-\boldsymbol{\xi}_{p1}^{T}\boldsymbol{K}_{p1}\boldsymbol{\xi}_{p1}+\frac{1}{\gamma_3}\tilde{m}\dot{\hat{m}}-\tilde{m}\boldsymbol{y}_2^{T}\bar{\boldsymbol{\vartheta}}_p+\tilde{\boldsymbol{\eta}}_p^{T}\boldsymbol{\Gamma}_4^{-1}\dot{\hat{\eta}}_p+\boldsymbol{y}_2^{T}\bar{\boldsymbol{f}}_d-\boldsymbol{y}_2^{T}\tanh\left(\frac{\boldsymbol{y}_2}{\varepsilon}\right)\hat{\boldsymbol{\eta}}_p+\boldsymbol{\xi}_{p1}^{T}\boldsymbol{K}_{p21}\boldsymbol{\xi}_{p2}-\frac{(1+k_p)\left\|\boldsymbol{y}_2\right\|^2}{\left\|\boldsymbol{y}_2\right\|^2+b_{p2}}\left|\boldsymbol{\xi}_{p1}^{T}\boldsymbol{K}_{p21}\boldsymbol{\xi}_{p2}\right|+\frac{1}{b_p}k_p\dot{k}_p \tag{82}$$

According to Lemma 1, we have

$$\boldsymbol{y}_2^{T}\bar{\boldsymbol{f}}_d\leqslant\boldsymbol{y}_2^{T}\tanh\left(\frac{\boldsymbol{y}_2}{\varepsilon}\right)\boldsymbol{\eta}_p+\frac{\left\|\boldsymbol{\varphi}_p\right\|^2}{2}+\frac{\left\|\boldsymbol{\eta}_p\right\|^2}{2} \tag{83}$$

where $\boldsymbol{\varphi}_p=[\varsigma\varepsilon,\varsigma\varepsilon,\varsigma\varepsilon]^{T}$.

Applying to the property of projection operator, the following inequality holds

$$\frac{1}{\gamma_3}\tilde{m}\dot{\hat{m}}-\tilde{m}\boldsymbol{y}_2^{T}\bar{\boldsymbol{\vartheta}}_p\leqslant 0 \tag{84}$$

In virtue of Eqs.(83) and (84), substituting Eqs.(78) and (80) into Eq.(82), we have

$$\dot{V}_4=-\boldsymbol{y}_1^{T}\boldsymbol{K}_3\boldsymbol{y}_1-\boldsymbol{y}_2^{T}\boldsymbol{K}_4\boldsymbol{y}_2-\boldsymbol{\xi}_{p1}^{T}\boldsymbol{K}_{p1}\boldsymbol{\xi}_{p1}-k_p\tilde{\boldsymbol{\eta}}_p^{T}\hat{\boldsymbol{\eta}}_p+\frac{\left\|\boldsymbol{\varphi}_p\right\|^2}{2}+\frac{\left\|\boldsymbol{\eta}_p\right\|^2}{2} \tag{85}$$

From Schwartz inequality, the following inequality can be obtained

$$-k_p\tilde{\boldsymbol{\eta}}_p^{T}\hat{\boldsymbol{\eta}}_p\leqslant-\frac{k_p}{2}\left\|\tilde{\boldsymbol{\eta}}_p\right\|^2+\frac{k_p}{2}\left\|\boldsymbol{\eta}_p\right\|^2 \tag{86}$$

Hence, substituting Eq.(86) into Eq.(85), one has the following inequality

$$\dot{V}_4=-\boldsymbol{y}_1^{T}\boldsymbol{K}_3\boldsymbol{y}_1-\boldsymbol{y}_2^{T}\boldsymbol{K}_4\boldsymbol{y}_2-\boldsymbol{\xi}_{p1}^{T}\boldsymbol{K}_{p1}\boldsymbol{\xi}_{p1}-\frac{k_p}{2}\left\|\tilde{\boldsymbol{\eta}}_p\right\|^2+\psi_p \tag{87}$$

where $\psi_p=\dfrac{k_p}{2}\left\|\boldsymbol{\eta}_p\right\|^2+\dfrac{\left\|\boldsymbol{\varphi}_p\right\|^2}{2}+\dfrac{\left\|\boldsymbol{\eta}_p\right\|^2}{2}$.

From Eq.(87), the stabilization of the transformed relative position systems (9) and (63) is ensured, then the relative attitude error can be guaranteed within prescribed performance bounds in Eq.(54). The main result is summarized in the following theorem.

Theorem 2 Consider the relative position dynamic systems (8) and (9) under the control force constraint (12) with Assumption 1—3, the proposed controller (77), adaptation laws (78) and (80) can guarantee that all signals in the closed-loop system are uniformly ultimately bounded, and the relative position error remains within the prescribed performance bounds all the time.

3 Numerical Simulations

In this section, a simulation scenario is considered to show the effectiveness and superiority of the proposed adaptive prescribed performance control scheme. Assume the drag free satellite is flying in a low orbit with the altitude 260 km. Then, the orbit angular velocity of the test mass is obtained as $\omega_t = \sqrt{\mu / r_t^3}$.

The mass and the inertia matrix of the outer satellite are respectively assumed to be $m = 20$ kg and

$$J = \begin{bmatrix} 20 & 0.1 & 0.2 \\ 0.1 & 20 & 0.3 \\ 0.2 & 0.3 & 20 \end{bmatrix} \mathrm{kg \cdot m^2}$$

The initial relative position and attitude are respectively characterized by

$$\begin{cases} \boldsymbol{r}_e(0) = [0.03, -0.05, 0.03]^{\mathrm{T}} \mathrm{m} \\ \boldsymbol{v}_e(0) = [0.15, -0.5, 0.1]^{\mathrm{T}} \mathrm{m/s} \\ \boldsymbol{\sigma}_e(0) = [-0.3, 0.4, 0.3]^{\mathrm{T}} \\ \boldsymbol{\omega}_e(0) = [0.01, -0.02, 0.01]^{\mathrm{T}} \mathrm{rad/s} \end{cases}$$

The disturbance force and torque are respectively modeled as

$$\boldsymbol{f}_d = \begin{bmatrix} 0.001 + 0.007\sin(\omega_t t) - 0.003\cos(\omega_t t) \\ 0.008 - 0.005\sin(\omega_t t) + 0.002\cos(\omega_t t) \\ -0.01 + 0.005\sin(\omega_t t) - 0.001\cos(\omega_t t) \end{bmatrix}$$

and

$$\boldsymbol{\tau}_d = \begin{bmatrix} 0.001 - 0.0008\sin(\omega_t t) + 0.0003\cos(\omega_t t) \\ 0.0008 - 0.0006\sin(\omega_0 t) - 0.0002\cos(\omega_0 t) \\ 0.001 + 0.0005\sin(\omega_t t) + 0.0001\cos(\omega_t t) \end{bmatrix}$$

The control magnitude constraints are selected as $f_{\max} = 10$ N and $\tau_{\max} = 5$ N · m. The parameters of control law, updating law, command filter and auxiliary system are set as shown in Table 1.

Choosing the chosen parameters of predefined performance bounds δ_{ui}, δ_{li} as $\delta_{ui} = \delta_{li} = 1$. The prescribed performance functions for relative position and attitude systems are respectively selected as

$$\rho_p(t) = (0.55 - 0.001)\mathrm{e}^{-0.2t} + 0.001$$

and

$$\rho_\sigma(t) = (0.90 - 0.001)\mathrm{e}^{-0.2t} + 0.001$$

In order to show the effectiveness of the proposed control scheme, the following comparative simulations are carried out.

Case 1 The control design with and without using the prescribed performance technique.

In order to give an fair comparison, all related gains and initial conditions are chosen exactly the same. The simulation results are demonstrated in Figs. 1—6, and the steady errors of relative states are tabulated in Table 2. It can be clearly seen in

Table 1 Control, update and command filter parameters

Notation	Value	Notation	Value
$\boldsymbol{K}_1$	$\boldsymbol{I}_3$	$\boldsymbol{K}_2$	$1.5\boldsymbol{I}_3$
$\boldsymbol{K}_3$	$2\boldsymbol{I}_3$	$\boldsymbol{K}_4$	$2\boldsymbol{I}_3$
$\boldsymbol{K}_{\sigma 1}$	$\boldsymbol{I}_3$	$\boldsymbol{K}_{\sigma 21}$	$\boldsymbol{I}_3$
$\boldsymbol{K}_{\sigma 2}$	$2\boldsymbol{I}_3$	$\boldsymbol{K}_{p1}$	$\boldsymbol{I}_3$
$\boldsymbol{K}_{p21}$	$\boldsymbol{I}_3$	$\boldsymbol{K}_{p2}$	$2\boldsymbol{I}_3$
$\boldsymbol{\Gamma}_1$	$0.01\boldsymbol{I}_6$	$\boldsymbol{\Gamma}_2$	$0.01\boldsymbol{I}_3$
γ_3	1	$\boldsymbol{\Gamma}_4$	$0.01\boldsymbol{I}_3$
k_σ	0.001	k_p	0.001
b_σ	0.001	$b_{\sigma 1}$	0.001
$b_{\sigma 2}$	0.1	b_p	0.001
b_{p1}	0.75	b_{p2}	0.1
ω_n	15	ζ	0.707

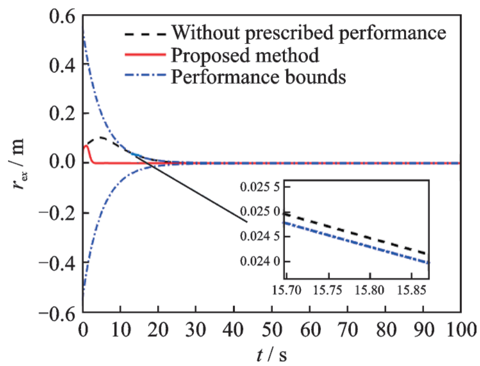

Fig.1 Relative position r_{ex}

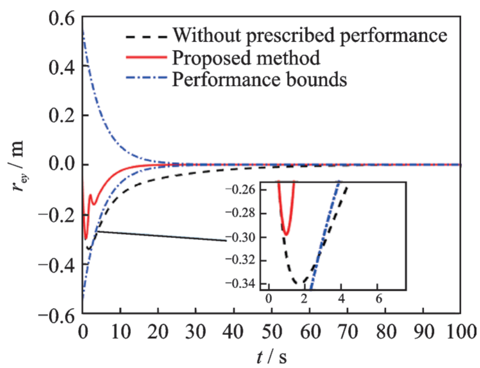

Fig.2 Relative position r_{ey}

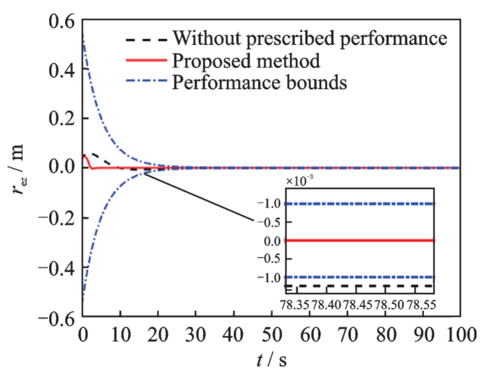

Fig.3 Relative position r_{ez}

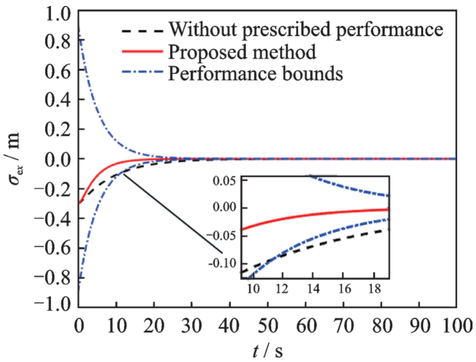

Fig.4 Relative attitude σ_{ex}

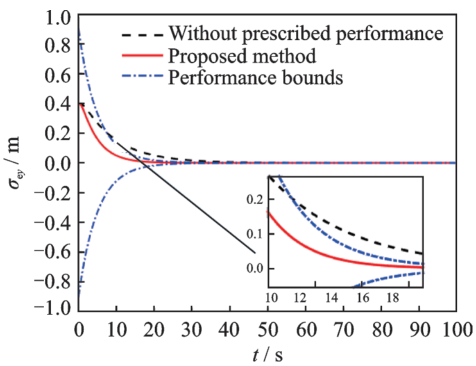

Fig.5 Relative attitude σ_{ey}

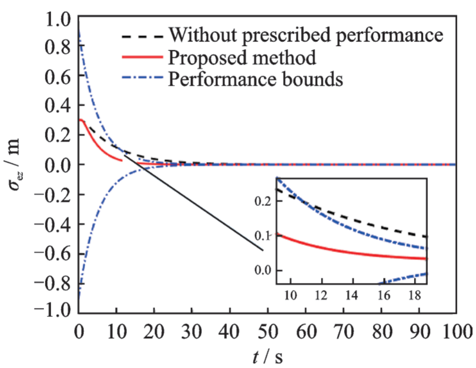

Fig.6 Relative attitude σ_{ez}

Table 2 Steady errors comparison

Index	Without prescribed performance	Proposed method
r_{ex}/m	1×10^{-4}	4×10^{-10}
r_{ey}/m	1×10^{-4}	1.453×10^{-8}
r_{ez}/m	1.2×10^{-3}	4.22×10^{-9}
σ_{ex}	1.097×10^{-4}	1.991×10^{-6}
σ_{ey}	5.55×10^{-5}	4.422×10^{-6}
σ_{ez}	1.13×10^{-4}	2.832×10^{-6}

Figs.1—6 that the time histories of the relative position and attitude obtained by the proposed method remain within the prescribed performance bounds for all time. However, the relative states for the case of without utilizing prescribed performance technique violate the predefined performance bounds and can not achieve the good performance of both transient error and steady error as this work.

Case 2 The control design with and without considering the actuator saturation. Figs.7—12 show the comparison between control forces with saturation and without saturation constraints, and the comparison between control torques with saturation and without saturation constraints, respectively. It is demonstrated that the control forces and control torques for the scenario without considering the actuator saturation exceed the actuator magnitude constraints during the initial transient phase, while the actuator capacity constraints are never violated for

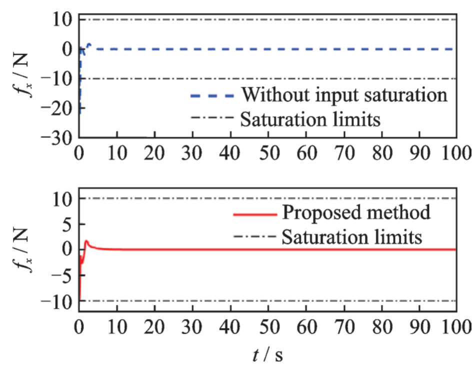

Fig.7 Control force f_x

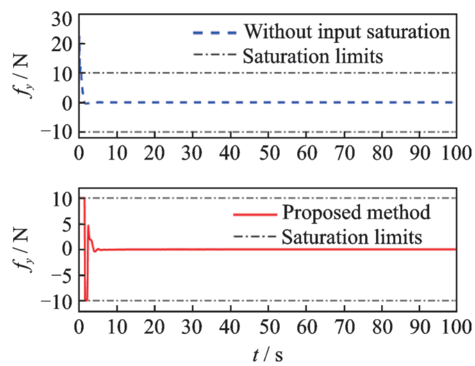

Fig.8 Control force f_y

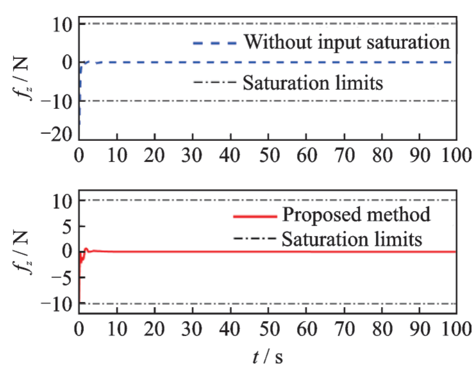

Fig.9 Control force f_z

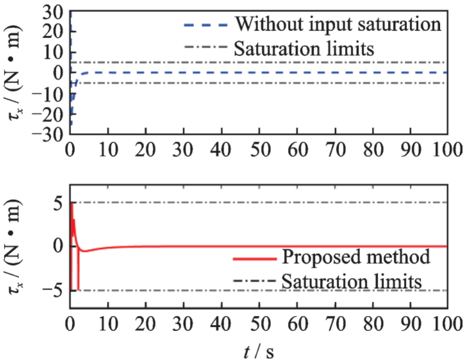

Fig.10 Control torque τ_x

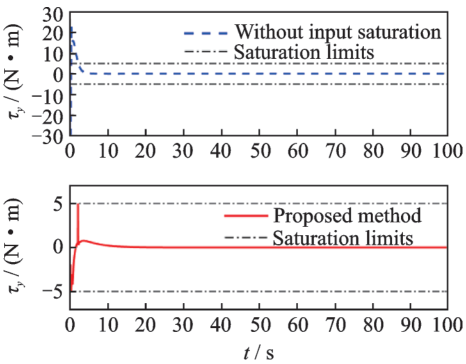

Fig.11 Control torque τ_y

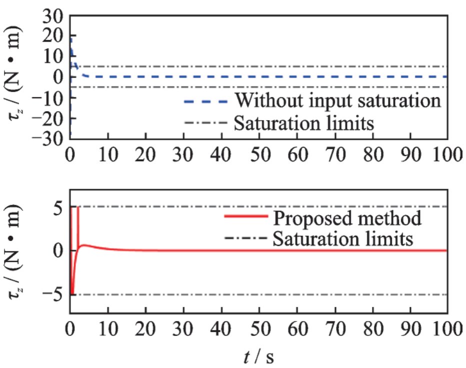

Fig.12 Control torque τ_z

the proposed method.

4 Conclusions

A relative position and attitude control strategy with prescribed performance is proposed for drag-free satellite with cubic test mass in the presence of model uncertainty, external disturbance and actuator saturation. The prescribed performance control technique is utilized to ensure that the relative position and attitude control error remain within the required performance constraints. Then, the command filter is applied to avoid the arduous analytic computations of the time derivative of virtual controls, and a novel auxiliary system is designed to tackle the problem of actuator saturation. Comparative numerical simulations are finally conducted to demonstrate the effectiveness and superiority of the proposed control scheme.

References

[1] PUGH G E. Proposal for a satellite test of the coriolis predictions of general relativity[M]//Nonlinear Gravitodynamics: The Lense-Thirring Effect. [S.l.]:[s.n.], 2003: 414-426.

[2] LANGE B O. The control and use of drag-free satellites[D]. Santa Clara, USA: Stanford University, 1964.

[3] TOUBOUL P, FOULON B, LAFARGUE L, et al. The microscope mission[J]. Acta Astronautica, 2002, 50(7): 433-443.

[4] MESTER J, TORII R, WORDEN P, et al. The STEP mission: Principles and baseline design[J]. Classical and Quantum Gravity, 2001, 18(13): 2475.

[5] SUMNER T J, ANDERSON J, BLASER J P, et al. STEP (satellite test of the equivalence principle)[J]. Advances in Space Research, 2007, 39(2): 254-258.

[6] BENCZE W J, DEBRA D B, HERMAN L, et al. On-orbit performance of the Gravity Probe B drag-free translation control system[C]//29th Guidance and Control Conference. Breckenridge, Colorado: American Astronautical Society, 2006.

[7] LI J, BENCZE W J, DEBRA D B, et al. On-orbit performance of gravity probe B drag-free translation control and orbit determination[J]. Advances in Space Research, 2007, 40(1): 1-10.

[8] GATH P, SCHULTE H R, WEISE D, et al. Drag free and attitude control system design for the LISA science mode[C]//AIAA Guidance, Navigation and Control Conference and Exhibit.[S.l.]: AIAA, 2007: 6731.

[9] GATH P, FICHTER W, KERSTEN M, et al. Drag free and attitude control system design for the LISA pathfinder mission[C]//AIAA Guidance, Navigation, and Control Conference and Exhibit. Rhode Island, USA: AIAA, 2004: 5430.

[10] MUZI D, ALLASIO A. GOCE: The first core Earth explorer of ESA's Earth observation programme[J]. Acta Astronautica, 2004, 54(3): 167-175.

[11] ALLASIO A, ANSELMI A, CATASTINI G, et al. GOCE mission: Design phases and in-flight experiences[J]. Advances in the Astronautical Sciences,

2010, 137(53): 2010.

[12] ZIEGLER B, BLANKE M. Drag-free motion control of satellite for high-precision gravity field mapping [C]//Proceedings of the International Conference on Control Applications. [S.l.]: IEEE, 2002, 1: 292-297.

[13] PRIETO D, BONA B. A modern approach to drag attenuation in a H/SUB/SPL infin//robust orbit control[C]//2004 International Conference on Information and Communication Technologies: From Theory to Applications. Damascus, Syria: IEEE, 2004: 315-316.

[14] PRIETO D, AHMAD Z. A drag free control based on model predictive techniques[C]//Proceedings of the 2005, American Control Conference. Portland, OR, USA: IEEE, 2005: 1527-1532.

[15] PETTAZZI L, LANZON A, THEIL S, et al. Design of robust drag-free controllers with given structure[J]. Journal of Guidance, Control, and Dynamics, 2009, 32(5): 1609-1621.

[16] CANUTO E. Embedded model control: Outline of the theory[J]. ISA transactions, 2007, 46(3): 363-377.

[17] CANUTO E. Drag-free and attitude control for the GOCE satellite[J]. Automatica, 2008, 44(7): 1766-1780.

[18] XU M, PAN X. Combined aerodynamic and orbital trajectories for partial drag-free flight at super-low altitudes[J]. Transactions of the Japan Society for Aeronautical and Space Sciences, 2017, 60(4): 235-243.

[19] CUI K, LIU H, JIANG W J, et al. Effects of cusped field thruster on the performance of drag-free control system[J]. Acta Astronautica, 2018, 144: 193-200.

[20] SCHAUB H, JUNKINS J L. Analytical mechanics of space systems[M]. USA: American Institute of Aeronautics and Astronautics, 2005.

[21] XIA K, HUO W. Robust adaptive backstepping neural networks control for spacecraft rendezvous and docking with input saturation[J]. ISA Transactions, 2016, 62: 249-257.

[22] ZHANG F, DUAN G R. Integrated translational and rotational finite-time maneuver of a rigid spacecraft with actuator misalignment[J]. IET Control Theory & Applications, 2012, 6(9): 1192-1204.

[23] POLYCARPOU M M, IOANNOU P A. A robust adaptive nonlinear control design[J]. Automatica, 1996, 32(3): 423-427.

[24] FARRELL J A, POLYCARPOU M, SHARMA M, et al. Command filtered backstepping[J]. IEEE Transactions on Automatic Control, 2009, 54(6): 1391-1395.

[25] HU J, ZHANG H. Immersion and invariance based command-filtered adaptive backstepping control of VTOL vehicles[J]. Automatica, 2013, 49(7): 2160-2167.

[26] BECHLIOULIS C P, ROVITHAKIS G A. Adaptive control with guaranteed transient and steady state tracking error bounds for strict feedback systems[J]. Automatica, 2009, 45(2): 532-538.

[27] POMET J B, PRALY L. Adaptive nonlinear regulation: Estimation from the Lyapunov equation[J]. IEEE Transactions on automatic control, 1992, 37(6): 729-740.

[28] HU Q, LI B, HUO X, et al. Spacecraft attitude tracking control under actuator magnitude deviation and misalignment[J]. Aerospace Science and Technology, 2013, 28(1): 266-280.

Authors Dr. **TAO Jiawei** is currently a Ph.D. candidate in Department of Automation at Tsinghua University. His research interests include spacecraft dynamics and control, nonlinear control and spacecraft formation flying.

Prof. **ZHANG Tao** is currently a professor in Department of Automation at Tsinghua University. He received his Ph.D. degree in Tsinghua University. His research interests are nonlinear system control theory and application, fault diagnosis and reliability analysis, intelligent control of robot, micro-satellite engineering and signal processing.

Author contributions Prof. **ZHANG Tao** contributed to the discussion and background of the study. Dr. **TAO Jiawei** designed the study, complied the models, conducted the analysis, interpreted the results and wrote the manuscript. Both authors commented on the manuscript draft and approved the submission.

Competing interests The authors declare no competing interests.

(Production Editor: Zhang Bei)